High Activation of Sb During Solid-Phase Epitaxy and Deactivation During Subsequent Thermal Process

Kunihiro Suzuki, *Senior Member, IEEE*, and Hiroko Tashiro

***Abstract*—Ion-implanted Sb is activated with higher concentrations than at thermal equilibrium during solid phase epitaxy, this Sb being deactivated at thermal equilibrium during the subsequent thermal process. It seems that Sb is trapped at the lattice sites at values above solid solubility during solid phase epitaxy and the diffusion of dopants degrades the resistance, as dopants begin to aggregate and deactivate. We showed that the onset of the increase in resistance is related to the diffusion length of Sb. By using a thermal process before deactivation, we could obtain shallow junctions with low resistance.**

***Index Terms*—Activation, anneal, deactivation, ion implantation, Sb, solid phase epitaxy.**

I. Introduction

THE SCALING theory requires shallow junctions with a decreasing gate length [1]–[4] and Sb is used to form such shallow junctions due to its sharp ion-implantation profiles and low-diffusion coefficient [5]–[7]. It has been reported that Sb is activated at lower temperatures [8] and for this reason we can fabricate shallow junctions with low resistance. Here, we investigate the phenomenon over a wide temperature range and clarify the mechanism to obtain highly activated Sb and the thermal budget required to maintain this low resistance.

II. Experiment

We used an Si (100) 10-Ωcm p-type substrate and implanted Sb ions with an energy of 5 keV and a dose of 5×10^{14} cm^{-2}. These substrates were subjected to various thermal processes. We evaluated the sheet resistance of the ion-implanted layer using a four-point probe, Sb concentration profiles using secondary ion mass spectrometry (SIMS), and amorphous layer thickness with a transmission electron microscope (TEM).

III. Results and Discussion

Fig. 1 shows the dependence of sheet resistance R on temperature, and Fig. 2 shows the dependence of R on time. R is almost constant between 600 and 900 °C for 1 s annealing, increases below 500 °C, and also increases in the temperature region exceeding 900 °C (Fig. 1). R decreases with time for low temperatures below 500 °C [Fig. 2(a)] while it increases at temperatures exceeding 800 °C [Fig. 2(b)]. R increases with time and then decreases at 1100 °C, and also at 700 °C for times longer than 5×10^4 s.

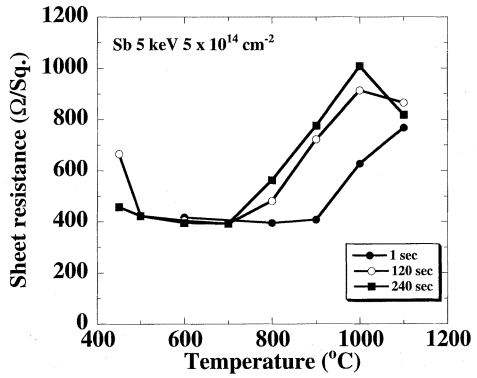

Fig. 1. Dependence of sheet resistance on temperature.

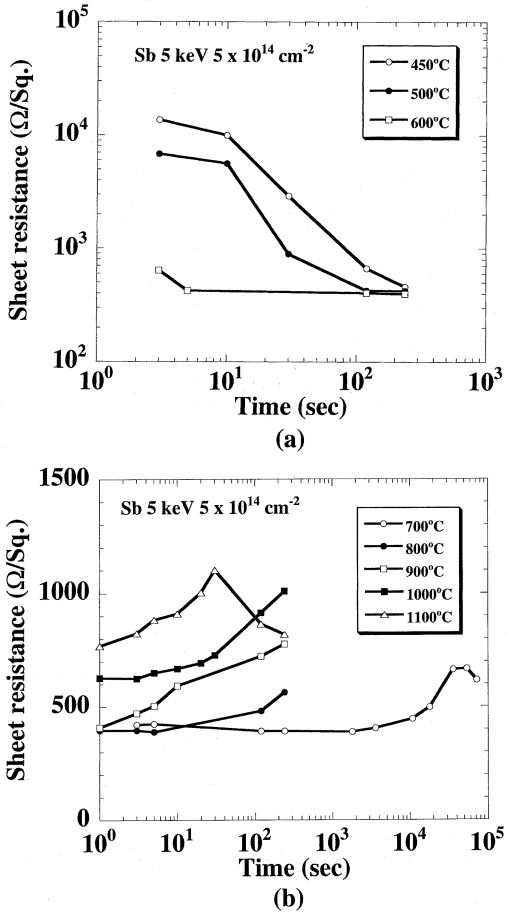

Fig. 2. Time evolution of sheet resistance. (a) 450, 500, and 600 °C. (b) 700, 800, 900, 1000, and 1100 °C.

We explain these events as follows.

The Sb ion implantation forms a continuous amorphous layer. In the early stages of the thermal process, solid phase

Manuscript received January 24, 20003; revised March 27, 2003. The review of this paper was arranged by Editor C.-Y. Lu.

The authors are with Fujitsu Laboratories Ltd., Atsugi, Kanagawa 243-01, Japan (e-mail: suzuki.kunihiro@jp.fujitsu.com).

Digital Object Identifier 10.1109/TED.2003.815136

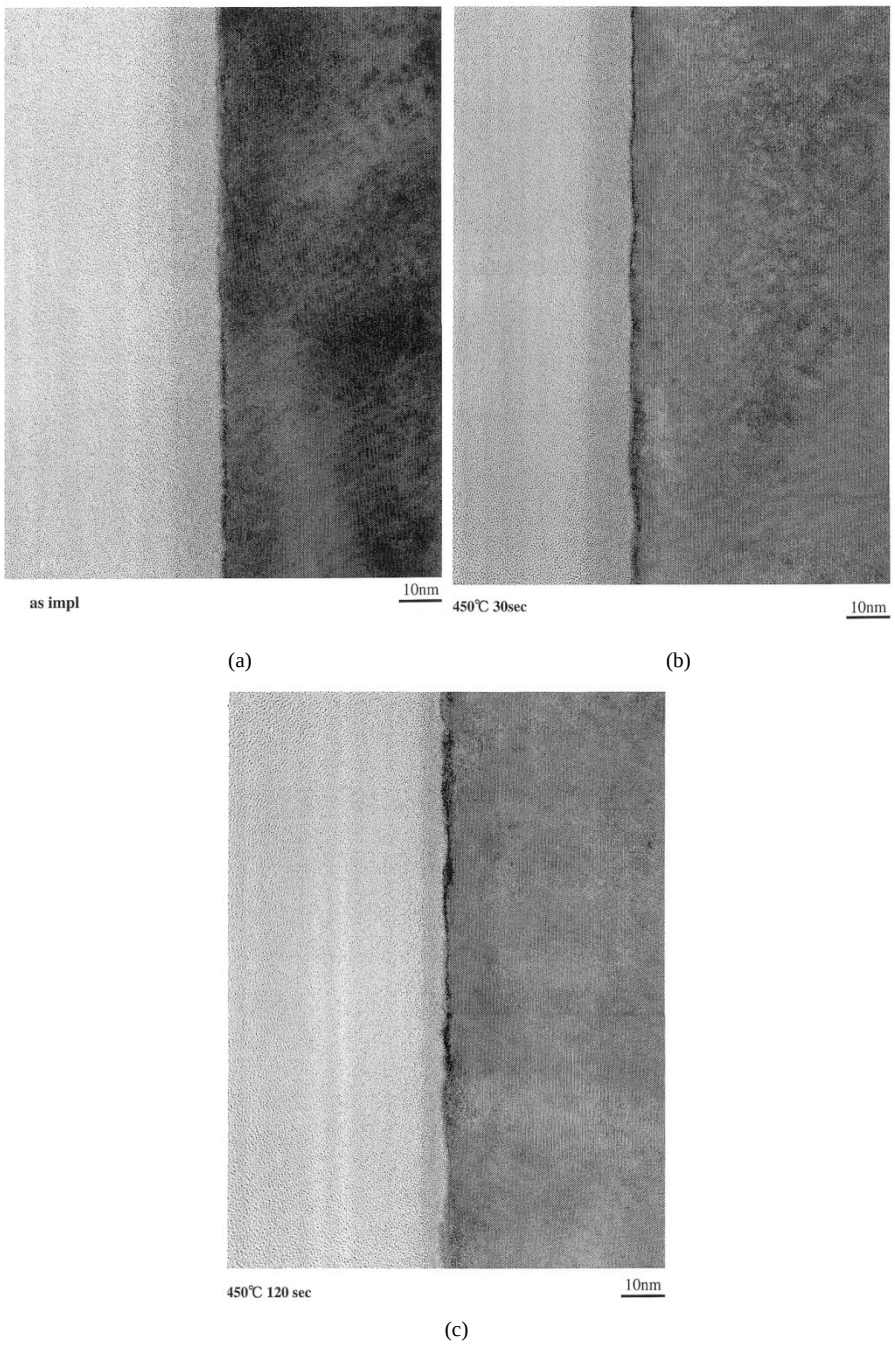

Fig. 3. TEM photomicrograph during solid phase epitaxy at 450 °C. (a) As impl. (b) 30 s. (c) 120 s.

epitaxy occurs and a higher Sb concentration is activated than at thermal equilibrium. The Sb diffuses to form clusters and the thermal equilibrium for solid solubility can be established after the chemical reaction that forms the clusters is completed. Therefore, this anomalous low resistance should be related to the quite high solid phase epitaxial speed rather than the diffusion speed.

Solid phase epitaxy gets underway temperatures as low as 450 °C. Therefore, the thickness of the low resistance layer increases with time and R decreases correspondingly. After the completion of solid phase epitaxial growth, the Sb diffuses and forms clusters and deactivation starts, resulting in an increased R. After the thermal equilibrium for clustering has been established, further diffusion results in an average lower doping concentration, and decreased R.

We will now verify the validity of the above model.

We evaluated the amorphous layer thickness by TEM. Fig. 3 is a TEM micrograph of samples annealed at 450 °C where a 10-nm-thick amorphous layer was formed after ion implantation and epitaxial regrowth. Fig. 4 shows the dependence of the amorphous layer thickness on time. The average regrowth rate was 0.038 nm/s, though it depends on the orientation, doping concentration, and dopant type [9]. Our extracted regrowth rate is within the reported values in Fig. 5.

We next evaluated the active Sb concentration in the regrowth layer.

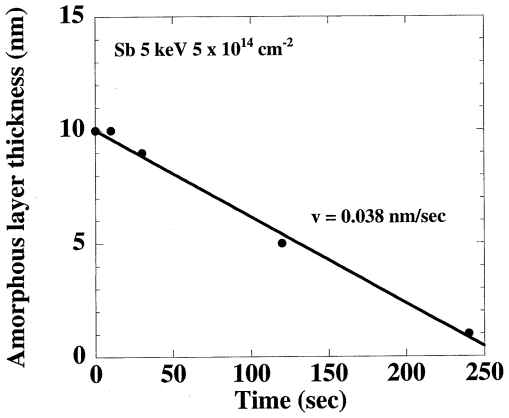

Fig. 4. Dependence of amorphous layer thickness on annealing time.

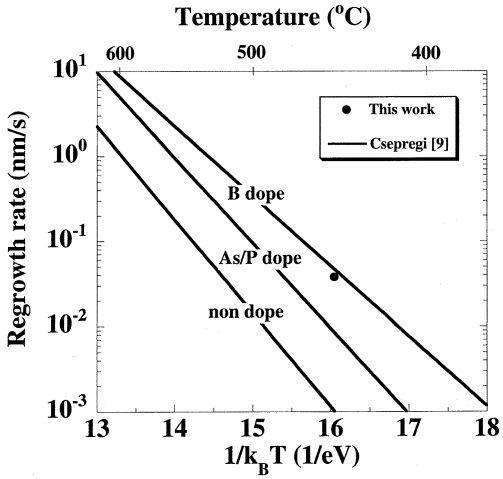

Fig. 5. Reported dependence of regrowth rate on temperature. Our extracted values are also shown.

Fig. 6 shows the as-implanted SIMS Sb profiles $\mathrm{N(x)}$. After regrowth was completed, we assumed that Sb had activated completely and had a maximum active concentration of $\mathrm{N_m}$. Therefore, the activated profile $\mathrm{N_{act}(x)}$ is

$$N_{\mathrm{act}}(x) = \begin{cases} N(x), & \text{for } N < N_m \\ N_m, & \text{for } N > N_m \end{cases} \tag{1}$$

which is indicated by the solid line in Fig. 6(a). If solid phase epitaxy is underway, $\mathrm{N_{act}}$ is given by

$$N_{\mathrm{act}}(x) \begin{cases} 0, & \text{in the amorphous layer} \\ Min[N(x),\, N_m], & \text{in the crystalline layer} \end{cases} \tag{2}$$

which is shown in Fig. 6(b). We verified the Sb profiles are almost the same as the implanted profile at temperatures below 600 °C with the time used in this experiment. Therefore, we used an implanted SIMS profile in (1) and (2). We have also assumed the same electron mobility as Arora *et al.* [10], which is

$$\mu_n = 88.3 + \frac{1241.8}{1 + \left(\frac{N_{act}}{1.295 \times 10^{17}}\right)^{0.891}} \left[\frac{cm^2}{Vs}\right] \tag{3}$$

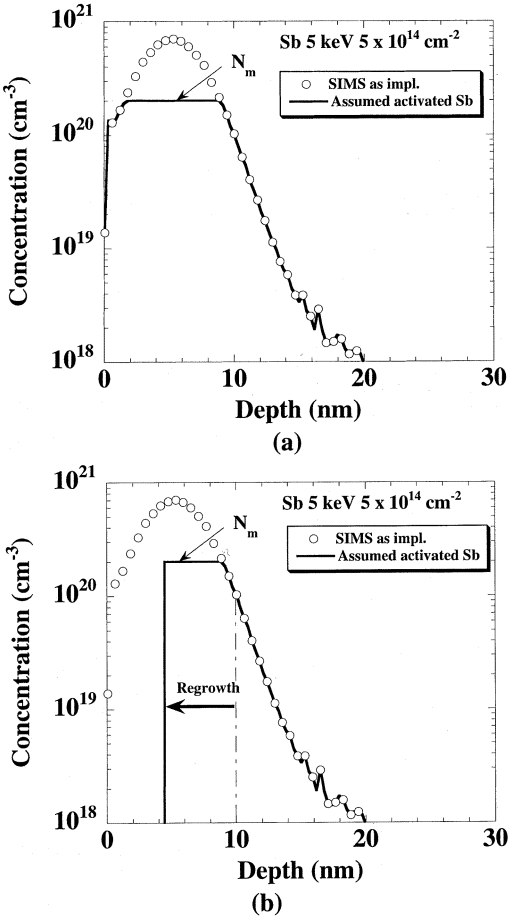

Fig. 6. Ion-implanted Sb profile and predicted active Sb concentration. (a) Completion of solid phase epitaxy. (b) Solid phase epitaxy is incomplete.

and R is

$$R = \frac{1}{\int eN_{act}\mu_n\, dx}. \tag{4}$$

The constant R independent of temperature is about 400 Ω/Sq., as shown in Fig. 1. In this region, we can assume that the crystal regrowth was completed while the diffusion of Sb is negligible. Therefore, we can evaluate the corresponding R using (1), (3) and (4) and identify $\mathrm{N_{max}}$. Fig. 7 shows the dependence of R on $\mathrm{N_m}$. An experimental R of around 400 Ω/Sq. in Fig. 1 is reproduced with an $\mathrm{N_m}$ of 2×10^{20} $\mathrm{cm^{-3}}$. This value is much larger than the reported values for the solid solubility of Sb [11], [12] as shown in Fig. 8. This means that a higher Sb concentration is activated than at thermal equilibrium, and the value is unaffected by temperature.

We have assumed that Sb is fully activated but the maximum value is $\mathrm{N_m}$ of 2×10^{20} $\mathrm{cm^{-3}}$ [Fig. 6(b)]. We evaluated the dependence of R on time using (2)–(4) (Fig. 3). Our model correlates well with experimental data as shown in Fig. 9 and the decrease of R is explained by the increase in thickness of the epitaxial layer.

Sb should diffuse to form clusters. When the diffusion length for Sb reaches the average distance for Sb to aggregate, R increases although we do not know what diffusion length is required for this. Therefore, we can use the diffusion length for the

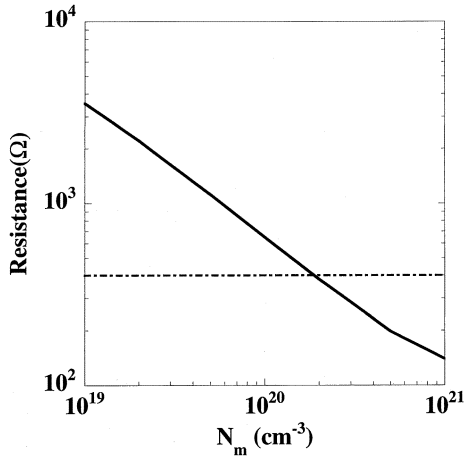

Fig. 7. Dependence of sheet resistance on N_m.

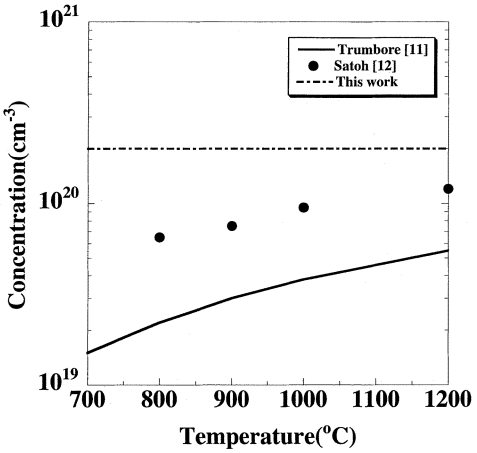

Fig. 8. Comparison of reported solid solubility of Sb at maximum active concentration during solid phase epitaxy.

criticism of the increase in R. This feature is exactly the same as those in [13]–[15], where impurities are activated at high temperatures and deactivation occurs during the subsequent lower temperature process.

The diffusion coefficient of Sb in Si is given by [6]

$$D = 1500 \exp\left[-\frac{4.80(eV)}{k_B T}\right] + \frac{n}{n_i} 13 \exp\left[-\frac{4.06(eV)}{k_B T}\right] \text{cm}^2/\text{s} \tag{5}$$

where n_i is the intrinsic carrier concentration, and given by [16]

$$n_i = 3.87 \times 10^{16} T^{1.5} \exp\left[-\frac{0.605(eV)}{k_B T}\right] \text{cm}^{-3} \tag{6}$$

n is the electron concentration. During the diffusion before the onset of the increase in R, we assume n is the maximum activated value of 2×10^{20} cm^{-3}.

The diffusion length L_D is defined by

$$L_D = 2\sqrt{Dt}. \tag{7}$$

Fig. 10 shows the dependence of the diffusion length on time for various temperatures. Resistance starts to increase when L_D is about 5 nm.

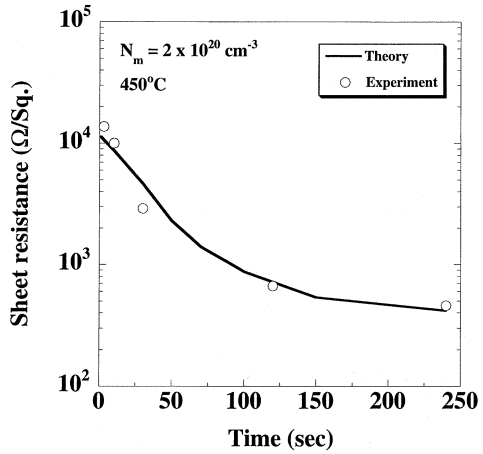

Fig. 9. Comparison of experimental sheet resistance on time with our model.

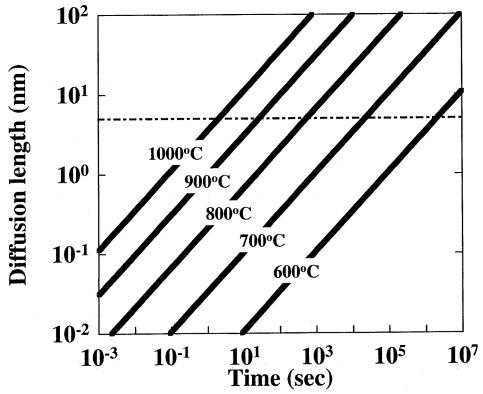

Fig. 10. Dependence of diffusion length on time.

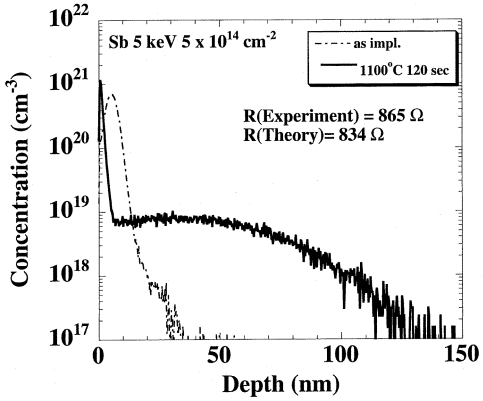

Fig. 11. Concentration profiles for Sb diffusion at 1100 °C.

The onset time for the resistance increase is 2×10^6 s for 600 °C, 2×10^4 s for 700 °C, 5×10^2 s for 800 °C, 25 s for 900 °C, and 2 s for 1000 °C (Fig. 10). This roughly corresponds to the time when R increases from 400 Ω/Sq. to around 550 Ω/Sq.

Fig. 11 shows diffusion profiles at 1100 °C for 120 s. The redistribution is significant, as was expected, and the estimated R is close to the value in Fig. 1. Therefore, the decrease of R after the increase due to deactivation can be explained by conventional diffusion, that is, the total amount of activated impurity increases. Furthermore, the average doping concentration

decreases, and the average mobility increases, resulting in a decrease in R with time.

IV. Summary

We investigated the activation and deactivation phenomenon of ion-implanted Sb. The Sb was activated with a higher concentration than at thermal equilibrium in the solid phase epitaxial layer before being deactivated during the subsequent thermal process. This deactivation is related to the formation of Sb clusters. We found that the increase in resistance is related to the diffusion coefficient of Sb, and that the corresponding onset time for deactivation can be evaluated as the diffusion length of about 5 nm. Using this thermal condition, we can obtain junctions and low resistance with higher activation than solid solubility.

Acknowledgment

The authors wish to thank H. Nakao for preparing samples, Y. Kataoka for SIMS measurement, and Y. Kodaka for TEM observation.

References

[1] R. H. Dennard, F. H. Gaensslen, H. Y. Yu, V. L. Rideout, E. Bassous, and A. L. Blanc, "Design of ion-implanted MOSFET's with very small physical dimensions," *IEEE J. Solid-State Circuits*, vol. SC-9, pp. 256–268, 1974.

[2] J. R. Brews, W. Fichtner, E. H. Nicollian, and S. M. Sze, "Generalized guide for MOSFET miniaturization," *IEEE Electron Device Lett.*, vol. EDL-1, pp. 2–4, 1980.

[3] P. Chattergee, W. R. Hunter, T. C. Holloway, and Y. T. Lin, "The impact of scaling laws on the choice of n-channels for MOS VLSIs," *IEEE Electron Device Lett.*, vol. EDL-1, pp. 220–223, 1980.

[4] G. Baccarani, M. R. Wordeman, and R. H. Dennard, "Generalized scaling theory and its application to a 1/4 micrometer MOSFET design," *IEEE Trans. Electron Devices*, vol. ED-31, pp. 452–462, 1984.

[5] K. Suzuki, A. Satoh, and T. Sugii, "Multiple Sb ion implantation technology for deep-submicron pMOS channel doping," *IEEE Trans. Electron Devices*, vol. 44, pp. 448–454, Mar. 1997.

[6] K. Suzuki, H. Tashiro, and T. Aoyama, "Sb diffusion in heavily doped Si substrates," *J. Electrochem. Soc.*, vol. 146, pp. 336–338, 1999.

[7] S. K. Ghandhi, *VLSI Fabrication Principles*. New York: Wiley, 1982, p. 132.

[8] H. Nakao, K. Okabe, T. Kubo, Y. Momiyama, and M. Kase, "Sub-10 nm depth ultra low resistance pn junction with antimony implantation," in *Proc. Int. Conf. Solid-State Devices Materials*, 2002, pp. 468–469.

[9] L. Csepregi, E. F. Kennedy, T. J. Gallagher, and J. W. Mayer, "Reordering of amorphous layers of Si implanted with ^{31}P, ^{75}As, and ^{11}B ions," *J. Appl. Phys.*, vol. 48, pp. 4234–4240, 1997.

[10] N. D. Arora, J. R. Haauser, and D. J. Roulston, "Electron and hole mobilities in silicon as a function of concentration and temperature," *IEEE Trans. Electron Devices*, vol. ED-29, pp. 292–295, 1982.

[11] F. A. Trumbore, "Solid solubilities of impurity elements in germanium and silicon," *Bell Syst. Tech. J.*, vol. 39, pp. 205–233, 1960.

[12] A. Satoh, K. Suzuki, H. Horie, and T. Horie, "Determination of solid solubility limit of In and Sb in Si using bonded silicon-on-insulator (SOI) substrate," in *Proc. Int. Conf. Microelectron. Test Structures*, 1995, pp. 259–263.

[13] H. Tashiro, K. Suzuki, T. Aoyama, and T. Miyashita, "Time evolution of boron-doped polycrystalline silicon gate resistance," *J. Electrochem.*, vol. 146, pp. 755–757, 1999.

[14] K. Suzuki, T. Hiroko, and T. Aoyama, "Time evolution of boron doped crystalline and polycrystalline silicon resistance," *J. Electrochem. Soc.*, vol. 147, pp. 3106–3108, 2000.

[15] K. Suzuki, T. Hiroko, and T. Aoyama, "Time evolution of arsenic, phosphorous, and boron-doped crystalline silicon resistance," *J. Electrochem. Soc.*, vol. 149, pp. G175–G178, 2002.

[16] F. J. Morin and J. P. Maita, "Electrical properties of silicon containing arsenic and boron," *Phys. Rev.*, vol. 96, pp. 28–35, 1954.

Kunihiro Suzuki (SM'01) was born in Aomori, Japan, in January 1959. He received the B.S., M.S., and Ph.D. degrees in electronics engineering from Tokyo Institute of Technology, Tokyo, Japan, in 1981, 1983, and 1996, respectively.

He joined Fujitsu Laboratories Ltd., Atsugi, Japan, in 1983 and has been engaged in design and modeling of high-speed bipolar and MOS transistors. He was a visiting researcher at the Swiss Federal Institute of Technology (ETH) Zurich, Switzerland, in 1996 and 1997, where he studied process modeling. His current interests are process and device modeling.

Hiroko Tashiro was born in Tokyo, Japan, in December 1960. She received the B.S. degree in mathematics from Tokai University, Kanagawa, Japan, in 1983.

She joined Fujitsu Laboratories Ltd., Atsugi, Japan, in 1983. Her current interest is device simulations.